ACS APPLIED MATERIALS & INTERFACES

Research Article

www.acsami.org

Highly Conducting, Transparent, and Flexible Indium Oxide Thin Film Prepared by Atomic Layer Deposition Using a New Liquid Precursor $Et_2InN(SiMe_3)_2$

Wan Joo Maeng,[†,⊗] Dong-won Choi,[‡,⊗] Kwun-Bum Chung,[§] Wonyong Koh,[∥] Gi-Yeop Kim,[⊥,#] Si-Young Choi,[⊥] and Jin-Seong Park*[,‡]

[†]Department of Materials Science and Engineering, University of Wisconsin−Madison, Madison, Wisconsin 53706, United States

[‡]Division of Materials Science and Engineering, Hanyang University, 222 Wangsimni-ro, Seongdong-gu, Seoul 133-719, Republic of Korea

[§]Department of Physics, Dongguk University, Seoul 100-715, Republic of Korea

[∥]UP Chemical, 81 Sandan-ro 197 beon-gil, Pyeongtaek-si, Gyeonggi-do 459-050, Republic of Korea

[⊥]Advanced Characterization & Analysis Group, Korea Institute of Materials Science, Changwon 642-831, Republic of Korea

[#]Department of Materials Science and Engineering, Pusan National University, Busan 609-735, Republic of Korea

Supporting Information

ABSTRACT: Highly conductive indium oxide films, electrically more conductive than commercial sputtered indium tin oxide films films, were deposited using a new liquid precursor $Et_2InN(SiMe_3)_2$ and H_2O by atomic layer deposition (ALD) at 225−250 °C. Film resistivity can be as low as 2.3×10^{-4}−5.16×10^{-5} Ω·cm (when deposited at 225−250 °C). Optical transparency of >80% at wavelengths of 400−700 nm was obtained for all the deposited films. A self-limiting ALD growth mode was found 0.7 Å/cycle at 175−250 °C. X-ray photoelectron spectroscopy depth profile analysis showed pure indium oxide thin film without carbon or any other impurity. The physical and chemical properties were systematically analyzed by transmission electron microscopy, electron energy loss spectroscopy, X-ray diffraction, optical spectrometer, and hall measurement; it was found that the enhanced electrical conductivity is attributed to the oxygen deficient InO_x phases.

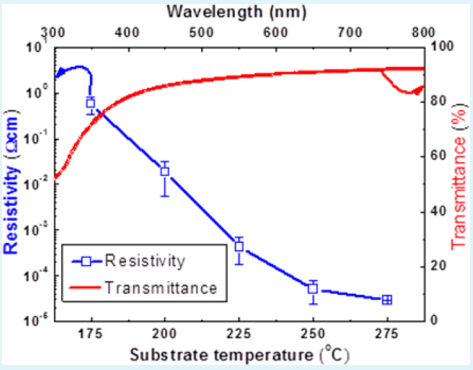

KEYWORDS: *indium oxide, atomic layer deposition, transparent conducting oxide, resistivity*

1. INTRODUCTION

Indium oxide thin films have been widely studied as transparent conducting oxides (TCOs),[1] thin-film transistors,[2] gas sensors,[3] and catalysts.[4] Among these various applications, there has been enormous interest in the next generation of see-through transparent electronics such as transparent thin-film transistors (TFTs) and organic light-emitting diodes (OLEDs) and photovoltaics.[5−7] To be used as transparent electrodes in these devices, TCOs require a high transmittance (>80%) in the visible region and low electrical resistivity, on the order of ≥10^{-3} Ω·cm.[8]

Indium oxide thin film is a very useful transparent conducting oxide material with a wide band gap. Indium oxide thin films have been deposited using a variety of methods including pulsed laser deposition,[9] sputtering,[10,11] and chemical vapor deposition.[12,13] However, many applications require precise control of film thickness, film composition, and low temperature deposition. For these properties, atomic layer deposition (ALD) has been used as a versatile film growth technique, because it enables the growth of uniform and high quality thin films with the precise control of the thickness and composition, as compared to other techniques.[14] In addition, the ALD process can deposit uniform and clean films on large areas at low processing temperatures due to self-limited surface reactions; hence, it can be applicable for transparent electrode deposition on future large-area electronics. For this reason, recently, the ALD deposition of TCO materials was widely studied, especially ZnO related materials such as Al, Ga, or Sn doped ZnO.[15−18] Researchers have reported good ALD growth characteristics; however, the resistivity is still not enough (>10^{-3} Ω·cm). In addition, from ref 15, the properties of ALD deposited film can be different. Thus, research of the ALD process using new precursors for different TCO materials is necessary

Among the various TCO materials, indium oxide ALD has been studied for the future microelectronic industry.[19−21] Unfortunately, all of these studies used solid In precursors, which have disadvantages of low vapor pressure and poor

Received: April 8, 2014
Accepted: September 26, 2014
Published: September 26, 2014

reproducibility, although some of them readily volatilize with mild heating. Indium oxide ALD using $InCl_3$ required too high of deposition temperature (~500 °C) and slow ALD growth (<0.3 Å/cycle) was observed.[22,23] The indium oxide ALD using indium acetylacetonate [$In(acac)_3$],[19] Indium-tris-guanidinates-[$In(iPr_2CNR_2)_3$],[24] and trimethylindium (TMIn) precursors[21,25] also showed slow ALD growth (<0.4 Å/cycle), and the film conductivity was poor (3×10^{-2} Ω·cm from $In(acac)_3$ and 2.8×10^{-3} Ω·cm from TMIn). The cyclopentadienylindium (InCp) precursor showed fast ALD growth (1.3 Å/cycle) at a proper ALD window (200−300 °C).[20,26,27] However, this precursor must be used with a strongly oxidizing reactant gas such as ozone (O_3), or with the simultaneous injection of H_2O and O_2. A high resistivity value (~1.6×10^{-2} Ω·cm) was also observed for an indium oxide thin film from InCp with ozone due to the removal of an intrinsic donor.[20] As an alternative, a liquid In precursor would by very advantageous in practical indium oxide thin-film processes, especially for deposition of low resistance indium oxide thin film and high growth rate.

In this study, we report on the microstructure, electrical, and optical properties of indium oxide films prepared using diethyl[bis(trimethylsilyl)amido]indium [$Et_2InN(TMS)_2$] as a liquid precursor for ALD. The deposited indium oxide thin films show reasonable ALD growth and ALD process window. Most of all, the deposited indium oxide films show electrically superior conductivity, being more conductive than commercial sputtered indium tin oxide (ITO) films while maintaining good optical transparency.

2. EXPERIMENTAL SECTION

The $Et_2InN(TMS)_2$ precursor was prepared according to previous literature[28] and supplied by UP Chemical Co., Ltd. (Pyeongtaek, Korea). For deposition of the indium oxide thin film, $Et_2InN(TMS)_2$ was used as an indium source and water vapor was used as a reactant gas. A homemade ALD system was employed for the deposition of indium oxide films on SiO_2 (100 nm thickness)/Si substrates. N_2 gas was used as purging gas as well as a carrier gases, whose inlets were separated on the side of the chamber. The N_2 gas flow rate (20 sccm) was controlled by a mass flow controller. $Et_2InN(TMS)_2$ was maintained at a temperature of 40 °C during vaporization. A typical ALD growth sequence for the indium oxide layers involved exposure to $Et_2InN(TMS)_2$ for 1 s, N_2 purging for 15 s, exposure to H_2O for 1 s, and N_2 purging for 15 s.

The 40 nm thick indium oxide thin films were deposited for various analyses, and measured by a spectral ellipsometer (SE, Woollam-VASE). Their resistivity, carrier concentration, and Hall mobility were investigated by means of Hall-effect measurement systems (HK5500PC (Accent Optical Technology) and an HMS 3000 (Ecopia Co.)) using a van der Pauw configuration. To reduce contact resistance, indium metal was used as the contact material at four rectangular sample edges. The microstructure of the films was studied by X-ray diffraction (XRD) (Rigaku diffractometer Ultima IV) using a Cu Kα X-ray source and transmission electron microscopy (TEM, JEOL JEM-2100 and JEOL JEM-2100F). In addition, to resolve the microstructure of the film more precisely, grazing incidence XRD (GI-XRD) was performed. The incidence angle, scan step size, and time per step during the GI-XRD measurement were 2°, 0.02°, and 1 s, respectively. Also, the films' chemical composition and chemical binding energy were investigated by X-ray photoelectron spectroscopy (XPS) (ESCA Lab 200R). The transmittance and band gap width were observed by ultraviolet−visible (UV−vis) spectroscopy (Optizen-3220 UV). Reflectivity and surface roughness were measured by optics spectrometry (USB4000-XR1) and atomic force microscopy (AFM, Park systems XE-70), respectively.

3. RESULTS AND DISCUSSIONS

Indium oxide thin films of 40 nm thicknesses were deposited on a SiO_2/Si substrate using an ALD technique because a less than 50 nm thick film was already used for the ALD TCO thin film.[21,27] The growth condition was studied by changing the precursor dosing time and substrate temperature. Figure 1a,b shows the ALD growth per cycle (GPC) as functions of $Et_2InN(TMS)_2$ dose and growth temperatures. Determination of dose can be obtained by using the ideal gas equation. From the vapor pressure of the precursor, we can obtain the mole amount of injected precursor from the canister, and obtain the adsorbed molecule number by dividing of the chamber surface. The detail method is described in elsewhere.[15] The ALD GPC increases rapidly with increasing dose. The GPC is saturated at ~0.7 Å/cycle above the precursor dose of 1×10^{-7} mol/cm^2. Also, the GPC is saturated 0.5 s of H_2O dosing time. (Figure S1, Supporting Information) The GPC values at temperatures from 150 to 275 °C are shown in Figure 1b. The ALD process window was found at 175−250 °C, and in that temperature region, the GPC remains almost constant. The GPC is almost 2 times larger than the previously reported indium oxide ALD using $InCl_3$, $In(acac)_3$, and TMIn. XPS depth profile indicated that small carbon impurities only existed on the surface, as shown in Figure 2a. After initial sputtering, the carbon impurity level was below the XPS detection limit, which is lower than 1%. Also, the Si content from the precursor $Et_2InN(TMS)_2$ was also below the XPS detection limit up to sputtering of the substrate before 5 min. This means that the Si from the precursor was fully eliminated during ALD. Figure 2b shows C

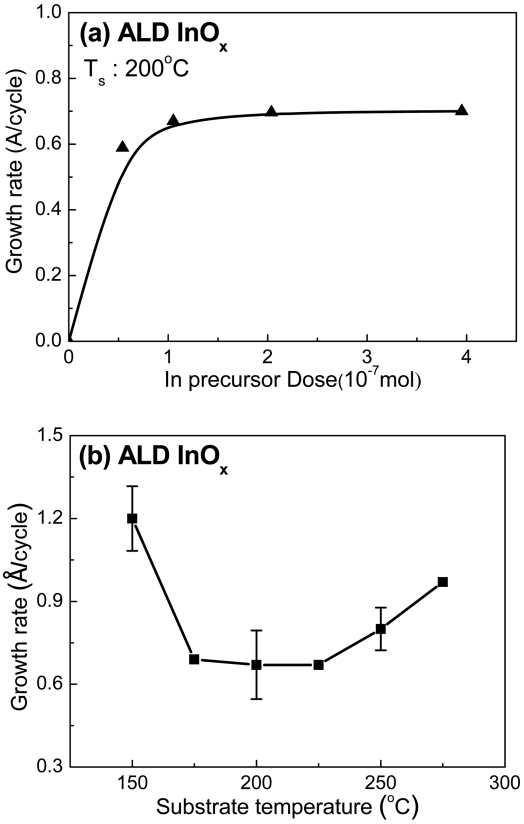

Figure 1. Dependence of growth rates of indium oxide deposited by ALD as a function of (a) precursor dose and (b) substrate temperature.

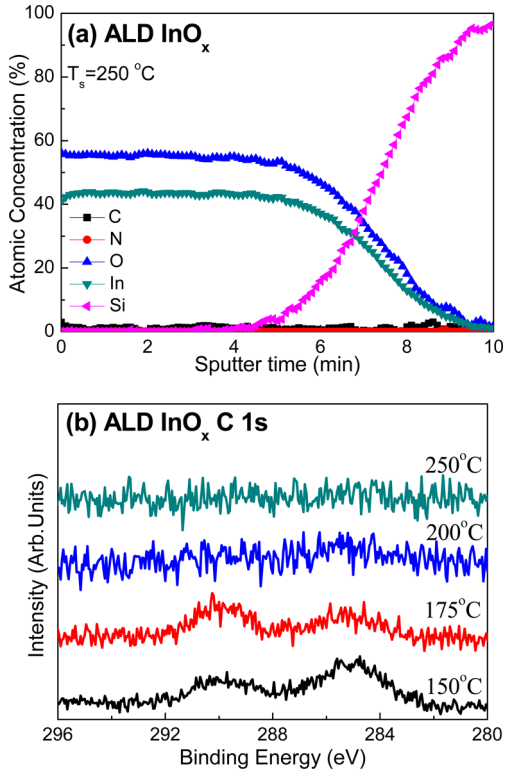

Figure 2. (a) Atomic concentration of In, O, C, N, Si of 250 °C deposited indium oxide thin film and (b) C 1s XPS spectra with deposition temperature.

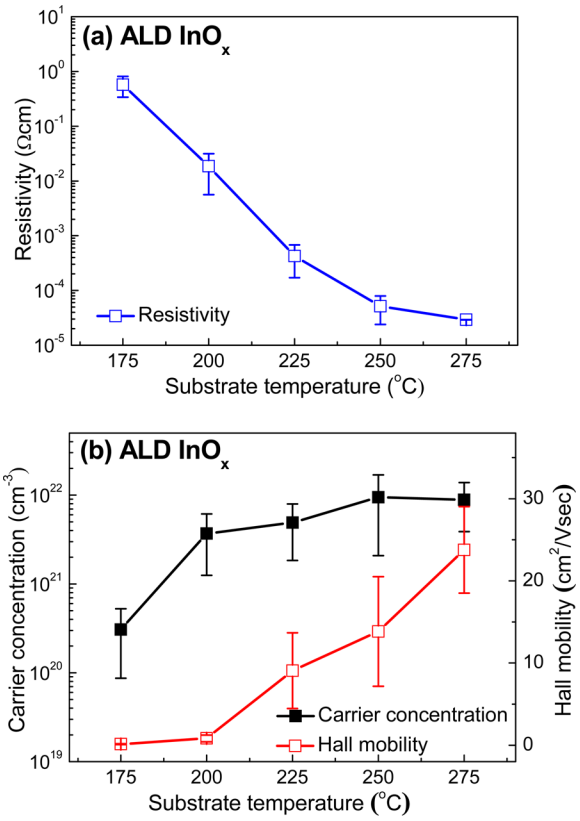

Figure 3. (a) Resistivity and (b) carrier concentration and Hall mobility data of ALD deposited indium oxide thin films as a function of growth temperature.

1s signals after surface sputtering are observed for the films deposited at different substrate temperatures. The C 1s signals are observed for the films deposited at 150 and 175 °C, but are absent for the films deposited at higher temperatures. This indicates that temperatures of 150 and 175 °C are too low for a complete ALD reaction without impurities.

Figure 3a,b shows the resistivity, carrier concentration, and Hall mobility of indium oxide films deposited at different temperatures. The resistivity of the film deposited at 200 °C showed a high resistance of 2×10^{-2} Ω·cm. However, the films' resistivity reduces continuously with increasing deposition temperature. As a result, the resistivity of the indium oxide film deposited at 250 °C is as low as 5.3×10^{-5} Ω·cm. In addition, the resistivity of a 100 nm thick film (7.2×10^{-5} Ω·cm) was very similar to that of a 40 nm thick film at 250 °C. This value is 1 or 3 orders of magnitude lower than the resistivity for a previously reported ALD indium oxide using other precursors,[19−23] or for indium oxide thin films formed by other deposition methods, such as sol−gel,[29] sputtering,[10,30] and chemical vapor deposition (CVD).[31,32] In addition, this film is more electrically conducting than commercial TCO materials such as ITO,[27] IZO,[33] Al:ZnO,[8] and even single-crystalline TCO materials.[34] Also, the film resistivity was saturated under the optimal deposition condition, which was sufficient doses of water (over 1 s) and indium precursor, as shown in Figure S2 (Supporting Information).

The carrier concentrations of the film deposited at 250 °C were measured to be as high as 9.3×10^{21} cm^{-3}, whereas those of indium oxide films deposited at lower temperatures were smaller, as low as 2×10^{20} cm^{-3} at 175 °C. The mobility was also as high as 13 cm^2/(V s) at the higher temperature of 250 °C and as low as 0.5 cm^2/(V s) at the lower temperature of 175 °C. This mobility is comparable to previously reported indium oxide thin films using ALD or other deposition methods, while carrier concentrations are almost 1−2 orders of magnitude higher.[10,13,21,26,35]

The evolution of crystallinity of the film deposited at 100−275 °C can be also observed in the XRD data shown in Figure 4. Under the 175 °C deposition temperature, the XRD result shows an amorphous phase, whereas indium oxide peaks start to appear at 200 °C; this parallels the TEM results. In addition, as the deposition temperature increases, the indium oxide (222) peak intensity is slightly increased and the additional peak is observed. Thus, better crystallinity at higher deposition temperature can explain the increase of electrical mobility.[36,37]

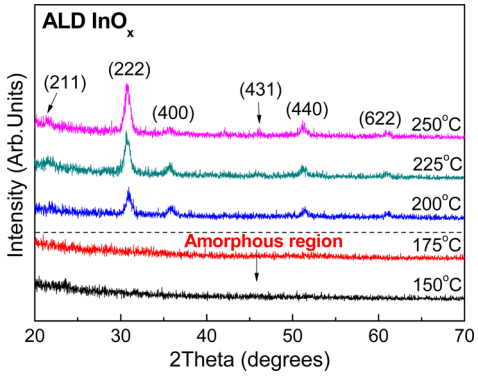

Figure 4. XRD data of indium oxide films deposited on silicon substrates, with different deposition temperatures.

dx.doi.org/10.1021/am502085c | ACS Appl. Mater. Interfaces 2014, 6, 17481−17488

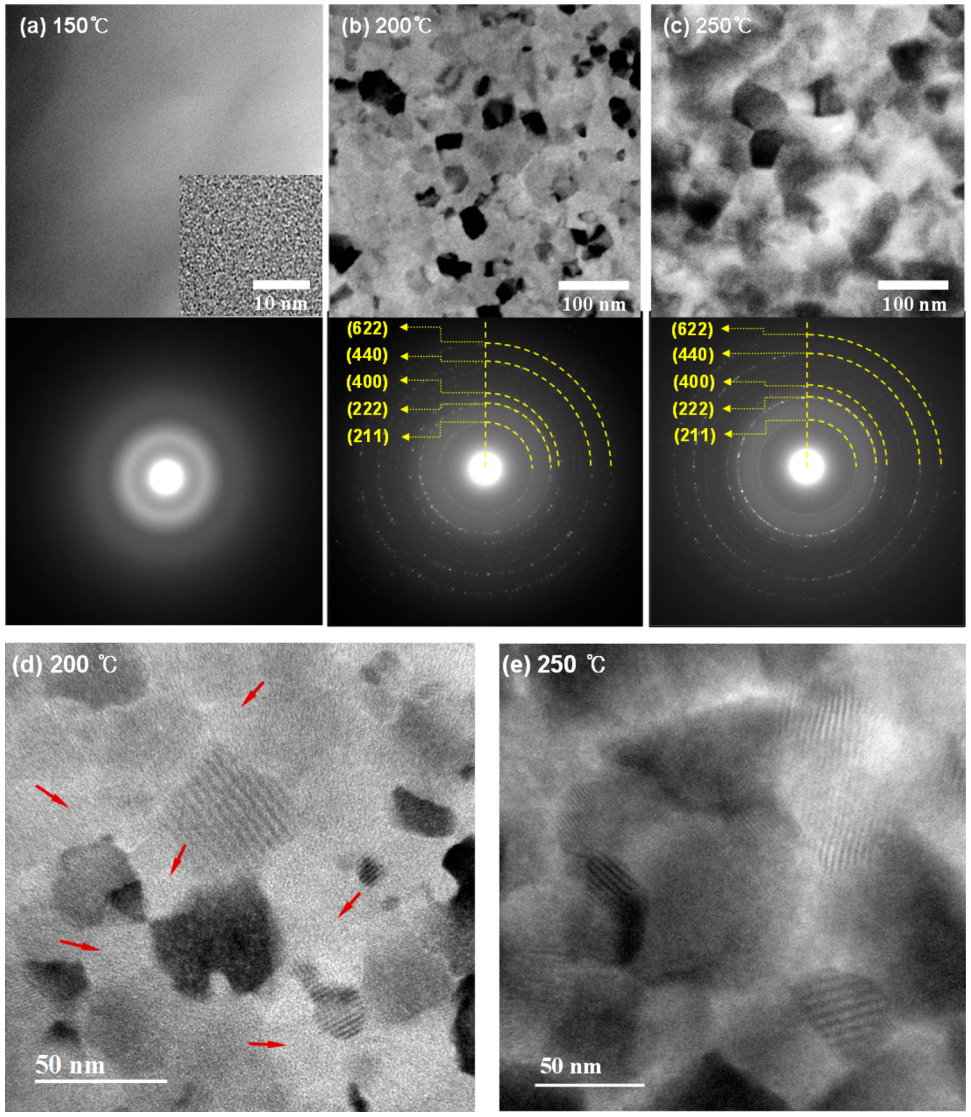

Figure 5. TEM images and SADP of indium oxide films deposited at (a) 150 °C (b and d) 200 °C, and (c and e) 250 °C. The red arrows in panel d indicate the amorphous phases.

The series of crystallinity behaviors mentioned above can be directly confirmed by TEM, as shown in Figure 5a−c, which shows the indium oxide films deposited at 150, 200, and 250 °C, respectively. The inset high resolution TEM image and selected area diffraction pattern (SADP) of Figure 5a indicate that the 150 °C deposited film is a fully amorphous phase. On the other hand, Figure 5b,c clarifies that the several nanometer crystalline phases appear in both the 200 and 250 °C deposited films, and the average crystalline size increases from ∼30 to ∼60 nm with the increase in deposition temperature. The (222) peak, supposedly the strongest one in SADP, is not present in the 150 °C deposited film, but appears in the film deposited at 200 °C and becomes even stronger in the 250 °C deposited one. The (440) SADP peak from the 250 °C deposited film is more continuous and stronger compared to the one from the 200 °C deposited film, which implies that the crystallinity was intensified by thermal activity. This explanation is again confirmed by Figure 5d,e, showing that the residual amorphous phases, indicated by the red arrows in the 200 °C deposited films, disappear altogether with the crystalline growth in the 250 °C deposited films. Therefore, the electron microscopic observations in this study confirm that, for the given conditions, an increase of deposition temperature effectively enhances the crystalline growth as well as the crystallinity of indium oxide film.

This increase of film crystallinity parallels with the increase of mobility observed for the films deposited at the same temperature range, as shown in Figure 3. To verify the crystallinity and the effect of oxygen vacancies, electron energy loss spectroscopy (EELS) was adopted, on the basis of its sensitivity to the electronic structural change, which is affected by vacancies, bonding state, and so on. The EELS system was equipped with probe-corrected JEM-2100F and analysis was performed under the scanning transmission electron microscopy (STEM) mode with a 3 mm collection aperture and 1.2 nm probe size, to improve EELS intensity. In Figure 6a,b, the oxygen K edges from the 150 and 200 °C deposited films appear similar to each other, which implies that the 200 °C deposited film is less crystallized, even though a crystalline structure is actually observed, as shown in Figure 5b,d.

However, Figure 6c, obtained from the 250 °C deposited film, shows a strong first peak in the oxygen K edge, which is

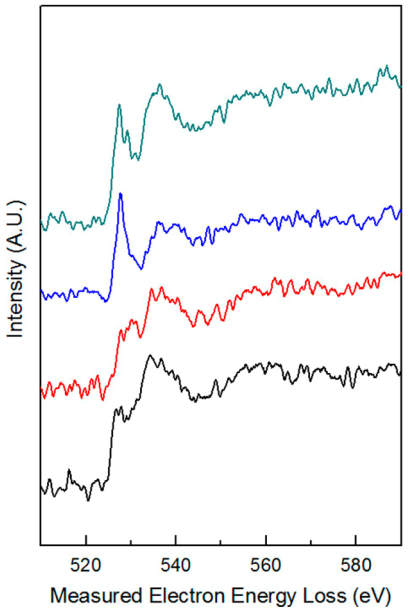

Figure 6. Oxygen K edge structures via EELS analysis obtained from indium oxide films deposited at (a) 150 °C, (b) 200 °C, and (c and d) 250 °C. The variation of the intensity ratio (I_{first}/I_{second}) is attributed to the existence of oxygen vacancies.

attributed to the stable oxygen and indium bonding state[38] Interestingly, 20 EELS data obtained from the 250 °C deposited film showed a significant variation in the first peak intensity whereas the EELS data from the 150 and 200 °C deposited films are all similar. Half of the EELS data from 250 °C exhibited the weak intensity ratio (I_{first}/I_{second}) of the first and second peaks; one of the representative data is shown in Figure 6d.

To understand the meaning of such variations in the oxygen K edge, the electronic structure of the oxygen K edge was calculated using the core−hole method and GGA PBE potential in CASTEP code (Figure S2, Supporting Information). It is quite challenging to achieve calculated results from core electronic structure calculations that are comparable to experimental data because limitations, such as the single electron model and nonrelativistic consideration in CASTEP code, have not been fully overcome yet.[39] However, the change in peak profiles can help determine which factor gives rise to the variation observed in the experimental EELS data. Figure S3 (Supporting Information), illustrating the calculated oxygen K edge of perfect indium oxide (black line) and defective indium oxide with oxygen vacancies (red line), indicates that the intensity ratio (I_{first}/I_{second}) of the first and second peaks is drastically decreased with the existence of oxygen vacancies. Therefore, the decreased I_{first}/I_{second} in half of total EELS data obtained from the 250 °C deposited film (Figure 6d) seems to be mainly caused by the oxygen vacancies.

Figure 7 shows the In 3d XPS data of four samples, used to investigate the indium chemical binding structure after surface sputtering to remove surface contaminant. The film deposited at 150 °C shows a symmetric single peak at 444.8 eV, corresponding to the In the $3d_{5/2}$ binding energy of indium oxide.[40] It indicates that all indium atoms are chemically bonded to oxygen, and thus exist as indium oxide in the film deposited at 150 °C. However, the XPS peaks appear at lower energies for films deposited at 200 and 250 °C. The In 3d peak was slightly shifted to a lower energy with the increase of

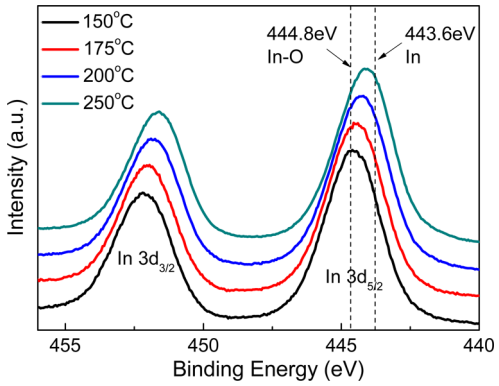

Figure 7. XPS results (In 3d peaks) of indium oxide films depending on deposition temperature.

growth temperature. In the 250 °C deposited films, the center energy of In $3d_{5/2}$ peaks are located at about 444 eV, which is almost 0.8 eV lower than the 150 °C deposited one. These results indicate that some of the indium atoms formed an oxygen deficient In oxide phase, because the XPS peak shifted slightly to the In metal bonding, whose binding energy peak appeared at 443.2 eV.[17]

Also, in Figure S4a−e (Supporting Information), the O 1s peak can be deconvoluted by In−O, oxygen deficient, and C−O or O−H bonding. As shown in Figure S4 (Supporting Information), the oxygen deficient bonding (O_2) is significantly increased. It is quite reasonable to compare this with the behavior of the In 3d XPS peak. From these XPS and EELS data, the excellent conductivity of the crystalline indium oxide films deposited at higher temperatures may be attributed to the presence of oxygen deficient InO_x bonding because these bonding states can generate electrons as a dopant.

This oxygen deficient InO_x might be induced by non-sufficient reaction between the precursor and reactant due to the low reactivity of H_2O. H_2O's relatively lower reactivity, compared to that of ozone or O_2 plasma of H_2O, was already reported in the study of ALD for gate oxide or capacitor oxide.[41] In other studies, the ozone or H_2O+O_2 was used as oxygen reactants for the ALD processing of In_2O_3 tin film using InCp, due to the low reactivity of H_2O.[20,26] However, the low reactivity of H_2O can enhance the conductivity by producing oxygen deficient InO_x. In the $In(acac)_2$ precursor case, the conductivity of In_2O_3 film from H_2O was much higher than when ozone was used.[19] This is the same result as reported in this paper. Using the ozone, we found that the resistivity of InO_x from $Et_2InN(TMS)_2$ was 2−3 times higher than that of H_2O. This indicates that ozone, comparing with H_2O, may suppress to generate oxygen deficient InO_x.

Figure 8 shows the transmittance of the samples, deposited at 100−250 °C. All films show over 80% transmittance in the range of 400−700 nm wavelengths. Especially, the transmittance of these InO_x films at the wavelength of 550 nm is as high as 89−91%, which is suitable for a transparent electrode. This is a comparable value with previous sol−gel and ALD deposited ITO thin films.[27,42] The inset of Figure 8 shows indium oxide thin films deposited on a flexible plastic substrate. The clean image of the alphabet indicates that this indium oxide thin film can be applicable for TCOs.

The films deposited at 175 °C and lower temperatures show a higher transmittance, over 90% in the range of 400−700 nm, whereas the films deposited at 200 °C and higher temperatures

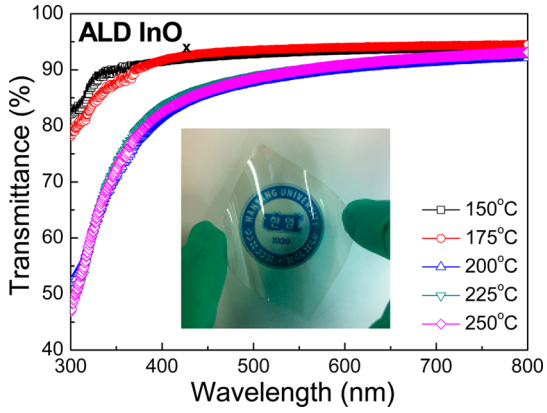

Figure 8. Transmittance data of six samples deposited at 150−250 °C after correction of transmittance of the glass substrate. The inset figure is a backside image of indium oxide thin films on a transparent plastic substrate.

show lower transmittance. The lower transmittance at higher growth temperatures may be related to crystallization. From the XRD data, the polycrystalline film is formed at 200 °C, which is the same temperature that coincides with the abrupt decrease of transmittance. From the refractive index (n) data, the n value was increased from 1.6 to 1.9 at 200 °C deposition temperature. (Figure S5, Supporting Information) The refractive index is related to film density and it is speculated that the dense films were formed by crystal formations. This refractive index change would be induced the reduction of transmittance. Another possible cause of the abrupt transmittance change is a change in surface roughness. However, the AFM data (Figure S6, Supporting Information) indicates the root-mean-square (RMS) surface roughness increased continuously from 0.4 to 2.9 nm. Thus, it cannot explain that the almost constant transmittance value over the 200 °C deposition temperature.

One more possibility is the presence of defects in the band gap of the films or changes of absorption spectra of In_2O_3 films deposited at 175 and 200 °C. To clarify sub-band edge states induced by defects such as carbon impurities incorporated at low deposition temperatures, SE analysis was carried out. As shown in Figure 9, there is an apparent difference in the absorption coefficient spectra for In_2O_3 films deposited between below 175 °C and over 200 °C. This difference

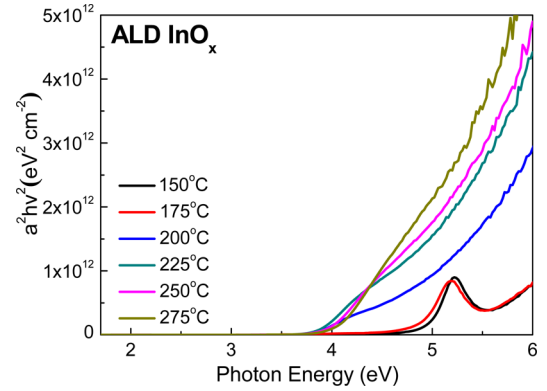

Figure 9. Tauc plot of the optical absorption coefficient against photon energy of In_2O_3 films deposited at 150−275 °C, measured by spectroscopic ellipsometry.

might be originated from carbon impurities incorporated at below 175 °C, and it influenced the poorly defined band edge. After carbon impurities are removed at over 200 °C, the relative area of absorption spectra increased drastically, and then gradually increased with increasing growth temperature. The larger relative absorption area is caused by the larger excitation of the carrier from the valence band to conduction band, which could lead to the easier charge transport within the conduction band due to the increase of unoccupied states.[43] This result correlates with the XPS (Figure 2b) and Hall measurement (Figure 3). The optical band gap under 175 °C deposited films cannot be determined by SE due to the poorly defined band edge, probably induced by defect related with carbon impurities incorporated at low deposition temperatures. On the other hand, the optical band gap of the films deposited at up to 200 °C are found 3.84−4.06 eV, which is comparable to previously reported ones.[44] The band gap remains the same for films deposited up to 250 °C and increases slightly further for the film deposited at 275 °C. The increase of band gap of the 275 °C sample, in spite of low resistivity and high carrier concentrations, can be explained by Burstein−Moss shift, which increases due to the filling up of low lying energy levels in the conduction band, leading to the shift of adsorption edge toward higher energy according to increasing carrier density.[43] However, this increment of band gap does not have any effect to transmittance. We can speculate from these results that the dominant transmittance degradation mechanism would be scattering by the film recrystallization rather than band gap change or other possibilities.

The origin of the superior conductive characteristics of this InO_x thin film should be understood more clearly, and on the basis of the above arguments, we propose a structural and transport model for the indium oxide thin films, as shown in Figure 10. The polycrystalline indium oxide films deposited using ALD with $Et_2InN(TMS)_2$ and water deposited over 200 °C show increased oxygen deficient bonding. A large amount of oxygen deficient bonding that acts like donors would be related to superior conductivity by generating carriers. The oxygen deficient InO_x may reside at grain boundaries because it is thermodynamically favorable.

Actually, this grain boundary segregation of oxygen vacancies has been observed for many other oxide materials such as $SrTiO_3$, HfO_2, and InSnO.[44−46] Generally, InO_x has a lot of oxygen deficient bonding, in Figure 7. The segregated oxygen deficient InO_x phase could increase the light scattering and help the conduction of electrons. The oxygen deficient InO_x enhanced the carrier concentration by up to 2 orders of magnitude because oxygen vacancy can act as carrier donation sites. Figure 10a shows these features: that the oxygen deficient InO_x donated carriers and, thermodynamically, the oxygen deficient InO_x are segregated near the grain boundary. In addition, this indium oxide thin film shows excellent conductivity, which would be induced by the oxygen deficient InO_x, which acts as a low scattering path between indium oxide grain boundaries. As a result, the carrier conduction is enhanced by reduction of grain boundary scattering. These mechanisms are shown at Figure 10b as a schematic diagram, and these two processes can be the possible model for the excellent conductivity of this InO_x thin film.

4. CONCLUSIONS

In summary, transparent indium oxide films with superior conductivity were prepared by ALD using $Et_2InN(TMS)_2$ as a

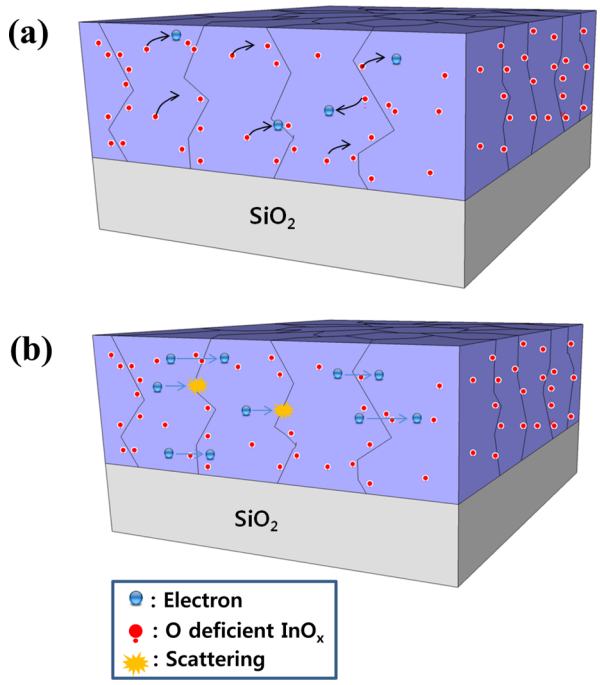

Figure 10. Schematic diagram of (a) grain boundary segregation of oxygen deficient InO_x and carrier generation, (b) electron transport without grain boundary scattering by oxygen deficient InO_x and with grain boundary scattering.

liquid precursor and H_2O. ALD growth per cycle was found to be 0.7 Å/cycle at deposition temperatures in the range 175–250 °C. The film resistivity is as low as 5.16×10^{-5} Ω·cm when deposited at 250 °C. Carrier concentration of the deposited films was found to be 1 or 2 orders of magnitude higher than indium oxide films of previous studies. In addition, over 80% transmittance in the range of 400–700 nm wavelengths was observed from all deposited films. These superior characteristics could be related to the grain boundary segregation of oxygen deficient InO_x atom, which can produce a high electron concentration, and the reduction of grain boundary scattering, with high transmittance. These superior TCO film properties and the equipment-friendly nature of the liquid $Et_2InN(TMS)_2$ precursor may be useful for applications in large area, high resolution and high speed displays in the near future.

■ ASSOCIATED CONTENT

Supporting Information

S1, Dependence of growth rates of indium oxide deposited by ALD as a function of H_2O dose; S2, resistivity of In_2O_3 film deposited at 250 °C (substrate temperature) as a function of the water dosing time; S3, calculated oxygen K edge structures of pristine (black) and defective (red) indium oxides. The calculation was performed through the core–hole method in CASTEP module. The significantly decreased first peak in oxygen K edge is attributed to the broken bonding state by the adjacent oxygen vacancy; S4, XPS results (O 1s peaks) of indium oxide films depending on deposition temperature; S5, refractive index of In_2O_3 thin films deposited 150, 175, 200, 225, 250, and 275 °C, respectively; S6, AFM results of InO thin films deposited 175, 200, 225, and 250 °C. The RMS roughness value showed with deposition temperature. It was continuously increased with increasing deposition temperature. This material is available free of charge via the Internet at http://pubs.acs.org.

■ AUTHOR INFORMATION

Corresponding Author

*J.-S. Park. E-mail: jsparklime@hanyang.ac.kr.

Author Contributions

⊗These two authors contributed equally to this work.

Notes

The authors declare no competing financial interest.

■ ACKNOWLEDGMENTS

This research was supported by UP Chemical and Korea Sanhak Foundation in 2012 and partially supported by the Global Frontier R&D Program through the Global Frontier Hybrid Interface Materials (GFHIM) of the National Research Foundation of Korea (NRF) funded by the Ministry of Science, ICT & Future Planning (2013M3A6B1078870 and 2013M3A6B1078872).

■ REFERENCES

(1) Tahar, R. B. H.; Ban, T.; Ohya, Y.; Takahashi, Y. Optical, Structural, and Electrical Properties of Indium Oxide Thin Films Prepared by the Sol-Gel Method. *J. Appl. Phys.* **1997**, *82*, 865–870.

(2) Zhang, H. Z.; Cao, H. T.; Chen, A. H.; Liang, L. Y.; Liu, Z. M.; Wan, Q. Enhancement of Electrical Performance in In_2O_3 Thin-Film Transistors by Improving the Densification and Surface Morphology of Channel Layers. *Solid-State Electron.* **2010**, *54*, 479–483.

(3) Korotcenkov, G.; Brinzari, V.; Cerneavschi, A.; Ivanov, M.; Golovanov, V.; Cornet, A.; Morante, J.; Cabot, A.; Arbiol, J. The Influence of Film Structure on In_2O_3 Gas Response. *Thin Solid Films* **2004**, *460*, 315–323.

(4) Gervasini, A.; Perdigon-Melon, J. A.; Guimon, C.; Auroux, A. an in-Depth Study of Supported In_2O_3 Catalysts for the Selective Catalytic Reduction of NOx: The Influence of the Oxide Support. *J. Phys. Chem. B* **2005**, *110*, 240–249.

(5) Park, J. S.; Maeng, W. J.; Kim, H. S.; Park, J. S. Review on Recent Developments in Amorphous Oxide Semiconductor Thin-Film Transistor Devices. *Thin Solid Films* **2012**, *520*, 1679–1693.

(6) Görrn, P.; Sander, M.; Meyer, J.; Kröger, M.; Becker, E.; Johannes, H. H.; Kowalsky, W.; Riedl, T. Towards See-through Displays: Fully Transparent Thin-Film Transistors Driving Transparent Organic Light-Emitting Diodes. *Adv. Mater.* **2006**, *18*, 738–741.

(7) Park, J. S.; Kim, K.; Park, Y. G.; Mo, Y. G.; Kim, H. D.; Jeong, J. K. Novel ZrInZnO Thin-Film Transistor with Excellent Stability. *Adv. Mater.* **2009**, *21*, 329–333.

(8) Maeng, W. J.; Lee, J. W.; Chung, K. B.; Park, J. S. Studies on Optical, Structural and Electrical Properties of Atomic Layer Deposited Al-Doped ZnO Thin Films with Various Al Concentrations and Deposition temperatures. *J. Phys. D: Appl. Phys.* **2011**, *44*, 445305–445305.

(9) Beena, D.; Lethy, K. J.; Vinodkumar, R.; Mahadevan Pillai, V. P.; Ganesan, V.; Phase, D. M.; Sudheer, S. K. Effect of Substrate Temperature on Structural, Optical and Electrical Properties of Pulsed Laser Ablated Nanostructured Indium Oxide Films. *Appl. Surf. Sci.* **2009**, *255*, 8334–8342.

(10) Cho, S. Effects of Rapid Thermal Annealing on the Properties of In_2O_3 Thin Films Grown on Glass Substrate by RF Reactive Magnetron Sputtering. *Microelectron. Eng.* **2012**, *89*, 84–88.

(11) Hotovy, I.; Pezoldt, J.; Kadlecikova, M.; Kups, T.; Spiess, L.; Breza, J.; Sakalauskas, E.; Goldhahn, R.; Rehacek, V. Structural Characterization of Sputtered Indium Oxide Films Deposited at Room Temperature. *Thin Solid Films* **2010**, *518*, 4508–4511.

(12) Girtan, M.; Folcher, G. Structural and Optical Properties of Indium Oxide Thin Films Prepared by an Ultrasonic Spray CVD Process. *Surf. Coat. Technol.* **2003**, *172*, 242–250.

(13) King, P. D. C.; Veal, T. D.; Fuchs, F.; Wang, C. Y.; Payne, D. J.; Bourlange, A.; Zhang, H.; Bell, G. R.; Cimalla, V.; Ambacher, O.;

Egdell, R. G.; Bechstedt, F.; McConville, C. F. Band Gap, Electronic Structure, and Surface Electron Accumulation of Cubic and Rhombohedral In_2O_3. *Phys. Rev. B* **2009**, *79*, 205211−205211.
(14) Kim, H.; Lee, H. B. R; Maeng, W. J. Applications of Atomic Layer Deposition to Nanofabrication and Emerging Nanodevices. *Thin Solid Films* **2009**, *517*, 2563−2580.
(15) Wu, Y.; Potts, S. E.; Hermkens, P. M.; Knoops, H. C. M.; Roozeboom, F.; Kessels, W. M. M. Enhanced Doping Efficiency of Al-Doped ZnO by Atomic Layer Deposition Using Dimethylaluminum Isopropoxide as an Alternative Aluminum Precursor. *Chem. Mater.* **2013**, *25*, 4619−4622.
(16) Yen, K. Y.; Chiu, C. H.; Hsiao, C. Y.; Li, C. W.; Chou, C. H.; Lo, K. Y.; Chen, T. P.; Lin, C. H.; Lin, T. Y.; Gong, J. R. Characteristics of GaN-based LEDs using Ga-Doped or In-Doped ZnO Transparent Conductive Layers Grown by Atomic Layer Deposition. *J. Cryst. Growth* **2014**, *387*, 91−95.
(17) Mullings, M. N.; Hägglund, C.; Tanskanen, J. T.; Yee, Y.; Geyer, S.; Bent, S. F. Thin Film Characterization of Zinc Tin Oxide Deposited by Thermal Atomic Layer Deposition. *Thin Solid Films* **2014**, *556*, 186−194.
(18) Maeng, W. J.; Park, J. S. Growth Characteristics and Film Properties of Gallium Doped Zinc Oxide Prepared by Atomic Layer Deposition. *J. Electroceram.* **2013**, *31*, 338−344.
(19) Nilsen, O.; Balasundaraprabhu, R.; Monakhov, E. V.; Muthukumarasamy, N.; Fjellvag, H.; Svensson, B. G. Thin Films of In_2O_3 by Atomic Layer Deposition Using $In(acac)_3$. *Thin Solid Films* **2009**, *517*, 6320−6322.
(20) Elam, J. W.; Martinson, A. B. F.; Pellin, M. J.; Hupp, J. T. Atomic Layer Deposition of In_2O_3 Using Cyclopentadienyl Indium: A New Synthetic Route to Transparent Conducting Oxide Films. *Chem. Mater.* **2006**, *18*, 3571−3578.
(21) Lee, D. J.; Kwon, J. Y.; Lee, J. I.; Kim, K. B. Self-Limiting Film Growth of Transparent Conducting In_2O_3 by Atomic Layer Deposition Using Trimethylindium and Water Vapor. *J. Phys. Chem. C* **2011**, *115*, 15384−15389.
(22) Asikainen, T.; Ritala, M.; Leskelä, M.; Prohaska, T.; Friedbacher, G.; Grasserbauer, M. AFM and STM Studies on In_2O_3 and ITO Thin Films Deposited by Atomic Layer Epitaxy. *Appl. Surf. Sci.* **1996**, *99*, 91−98.
(23) Mikko, R.; Timo, A.; Leskelä, M. Enhanced Growth Rate in Atomic Layer Epitaxy of Indium Oxide and Indium-Tin Oxide Thin Films. *Electrochem. Solid-State Lett.* **1998**, *1*, 156−157.
(24) Gebhard, M.; Hellwig, M.; Parala, H.; Xu, K.; Winter, M.; Devi, A. Indium-Tris-Guanidinates: A Promising Class of Precursors for Water Assisted Atomic Layer Deposition of In_2O_3 Thin Films. *Dalton Trans.* **2014**, *43*, 937−940.
(25) Ott, A. W.; Johnson, J. M.; Klaus, J. W.; George, S. M. Surface Chemistry of In_2O_3 Deposition using $In(CH_3)_3$ and H_2O in a Binary Reaction Sequence. *Appl. Surf. Sci.* **1997**, *112*, 205−215.
(26) Libera, J. A.; Hryn, J. N.; Elam, J. W. Indium Oxide Atomic Layer Deposition Facilitated by the Synergy between Oxygen and Water. *Chem. Mater.* **2011**, *23*, 2150−2158.
(27) Elam, J. W.; Baker, D. A.; Martinson, A. B. F.; Pellin, M. J.; Hupp, J. T. Atomic Layer Deposition of Indium Tin Oxide Thin Films Using Nonhalogenated Precursors. *J. Phys. Chem. C* **2008**, *112*, 1938−1945.
(28) Porchia, M.; Benetollo, F.; Brianese, N.; Rossetto, G.; Zanella, P.; Bombieri, A. G. Diethylindium(III) Derivatives: Synthesis and Characterization of Diethylindium(III) Dialkylamides and Diethylindium(III) Pyrrolide. X-ray Crystal Structures of Diethylindium(III) Pyrrolide and Diethylindium(III) Bromide. *J. Organomet. Chem.* **1992**, *424*, 1−13.
(29) Radhouane, B. H. T.; Takayuki, B.; Yutaka, O.; Takahashi, A. Y. Optical, Structural, and Electrical Properties of Indium Oxide Thin Films Prepared by the Sol-Gel Method. *J. Appl. Phys.* **1997**, *82*, 865−870.
(30) Kato, K.; Omoto, H.; Tomioka, T.; Takamatsu, A. Changes in Electrical and Structural Properties of Indium Oxide Thin Films through Post-Deposition Annealing. *Thin Solid Films* **2011**, *520*, 110−116.
(31) Chou, T. Y.; Chi, Y.; Huang, S. F.; Liu, C. S.; Carty, A. J.; Scoles, L.; Udachin, K. A. Fluorinated Aminoalkoxide and Ketoiminate Indium Complexes as MOCVD Precursors for In_2O_3 Thin Film Deposition. *Inorg. Chem.* **2003**, *42*, 6041−6049.
(32) Toshiro, M.; Kitamura, T. Plasma Metal Organic Chemical Vapor Deposition of Indium Oxide Thin Films. *Jpn. J. Appl. Phys.* **1989**, *28*, L1096−L1097.
(33) Ito, N.; Sato, Y.; Song, P. K.; Kaijio, A.; Inoue, K.; Shigesato, Y. Electrical and Optical Properties of Amorphous Indium Zinc Oxide Films. *Thin Solid Films* **2006**, *496*, 99−103.
(34) Kim, H. J.; Kim, U.; Kim, H. M.; Kim, T. H.; Mun, H. S.; Jeon, B. G.; Hong, K. T.; Lee, W. J.; Ju, C.; Kim, K. H.; Cha, K. High Mobility in a Stable Transparent Perovskite Oxide. *Appl. Phys. Express* **2012**, *5*, 061102−061102.
(35) Adurodija, F. O.; Izumi, H.; Ishihara, T.; Yoshioka, H.; Motoyama, M.; Murai, K. Influence of Substrate Temperature on the Properties of Indium Oxide Thin Films. *J. Vac. Sci. Technol., A* **2000**, *18*, 814−818.
(36) Lu, J. G.; Ye, Z. Z.; Zeng, Y. J.; Zhu, L. P.; Wang, L.; Yuan, J.; Zhao, B. H.; Liang, Q. L. Structural, Optical, and Electrical Properties of (Zn,Al)O Films over a Wide Range of Compositions. *J. Appl. Phys.* **2006**, *100*, 073714-1−073714-11.
(37) Masuda, S.; Kitamura, K.; Okumura, Y.; Miyatake, S.; Tabata, H.; Kawai, T. Transparent Thin Film Transistors using ZnO as an Active Channel Layer and Their Electrical Properties. *J. Appl. Phys.* **2003**, *93*, 1624−1630.
(38) Lai, C. W.; Dai, J. Y.; Zhang, X. Y.; Chan, H. L. W.; Xu, Y. M.; Li, Q.; Ong, H. C. In Situ Synthesis and Phase Transformation of In_2O_3/Sb Core-Shell Nanostructures. *J. Cryst. Growth* **2005**, *282*, 383−388.
(39) Mizoguchi, T.; Olovsson, W.; Ikeno, H.; Tanaka, I. Theoretical ELNES using One-Particle and Multi-Particle Calculations. *Micron* **2010**, *41*, 695−709.
(40) Hewitt, R. W.; Winograd, N. Oxidation of Polycrystalline Indium Studied by X-ray Photoelectron Spectroscopy and Static Secondary Ion Mass Spectroscopy. *J. Appl. Phys.* **1980**, *51*, 2620−2624.
(41) Maeng, W. J.; Kim, H. Thermal and Plasma-Enhanced ALD of High Quality Ta and Ti Oxide Thin Films from Alkylamide Precursors. *Electrochem. Solid-State Lett.* **2006**, *9*, G191−G194.
(42) Chen, Z.; Li, W.; Li, R.; Zhang, Y.; Xu, G.; Cheng, H. Fabrication of Highly Transparent and Conductive Indium−Tin Oxide Thin Films with a High Figure of Merit via Solution Processing. *Langmuir* **2013**, *29*, 13836−13842.
(43) Shuang, L.; Bi, X. Structure, Conductivity, and Transparency of Ga-Doped ZnO Thin Films Arising from Thickness Contributions. *J. Appl. Phys.* **2008**, *104*, 113533−113533.
(44) Klie, R. F.; Browning, N. D. Atomic Scale Characterization of Oxygen Vacancy Segregation at $SrTiO_3$ Grain Boundaries. *Appl. Phys. Lett.* **2000**, *77*, 3737−3739.
(45) Rauf, I. A. Structure and Properties of Tin-Doped Indium Oxide Thin Films Prepared by Reactive Electron-Beam Evaporation with a Zone-Confining Arrangement. *J. Appl. Phys.* **1996**, *79*, 4057−4065.
(46) McKenna, K.; Shluger, A. The Interaction of Oxygen Vacancies with Grain Boundaries in Monoclinic HfO_2. *Appl. Phys. Lett.* **2009**, *95*, 222111-1−222111-3.